Secondary Structures of *Escherichia coli* Antisense *micF* RNA, the 5′-End of the Target *ompF* mRNA, and the RNA/RNA Duplex†

Matthew Schmidt,‡ Ping Zheng,§ and Nicholas Delihas*,‡

Graduate Program in Genetics and Department of Molecular Genetics and Microbiology and Department of Chemistry, State University of New York at Stony Brook, Stony Brook, New York 11794

Received November 14, 1994; Revised Manuscript Received January 9, 1995⊗

ABSTRACT: The *Escherichia coli micF* RNA is a prototype for a class of antisense RNAs encoded by genes at different loci from those that code for their target RNAs. RNAs in this class exhibit only partial complementarity to their targets. *micF* RNA binds to and regulates the stability of *ompF* mRNA in response to a variety of environmental stimuli. The secondary structures of *micF* RNA, *ompF*-213 mRNA (a segment containing the 213 nucleotides at the 5′-terminus of the target message), and the *micF* RNA/*ompF*-213 mRNA duplex were analyzed *in vitro* by partial digestion with structure-specific ribonucleases and chemical modification. Both *micF* RNA and *ompF* mRNA have single-stranded 5′-ends and contain stable stem-loop structures. Strong phylogenetic support for the proposed secondary structure for *E. coli micF* RNA is provided by a comparison of structural models derived from *micF* sequences from related bacteria. The *micF* RNA/*ompF*-213 mRNA duplex interaction appears to involve only a short segment of *micF* RNA. Unfolding of only one stem-loop of *micF* RNA and a minor stem-loop of *ompF*-213 mRNA appears to be necessary to form the duplex. The probing data suggest that the Shine−Dalgarno sequence and AUG start codon of *ompF* mRNA, found in single-stranded regions in the free message, are base-paired to *micF* RNA in the RNA/RNA duplex.

Small RNAs have been shown to participate in a wide variety of cellular processes, and many of these molecules are antisense RNAs which regulate gene expression and other physiological functions (Inouye & Delihas, 1988). Antisense RNAs affect the function of complementary target RNAs by binding to their targets [for a comprehensive review, see Simons (1993)]. One group of antisense RNAs are encoded by genes that are located in different regions of the chromosome from the genes that encode their targets, and these regulatory RNAs are only partially complementary to their target RNAs (Delihas, 1995). In prokaryotes, two such unlinked antisense RNA genes have been characterized, *micF* (Mizuno et al., 1983,1984; Andersen et al., 1987) and *dicF* (Tetart & Bouche, 1992). In eukaryotes, *lin-4* codes for two small RNAs that regulate the expression of the cell fate determinant, LIN-14 protein (Lee et al., 1993). The regulatory RNA/target RNA interactions of these *trans*-encoded antisense RNAs pose an interesting and challenging problem of duplex formation and structure.

The *micF* gene codes for a 93 nucleotide RNA (Andersen et al., 1987) that posttranscriptionally regulates the expression of outer membrane protein F (OmpF) in *Escherichia coli* in response to temperature increase and a variety of other environmental stress conditions (Mizuno et al., 1984; Andersen et al., 1989; Ramani et al., 1994). The expression of *micF* is under the control of several regulons, and its regulation is part of a global response to various environmental stimuli (Mizuno et al., 1984; Aiba et al., 1987; Misra & Reeves, 1987; Cohen et al., 1988; Coyer et al., 1990; Rosner et al., 1991; Chou et al., 1993; Gidrol & Farr, 1993). The *micF* gene has also been identified in several Gram-negative bacterial species (Esterling & Delihas, 1994; Hutsul & Worobec, 1994). Thus the role of *micF* RNA in global responses of cells to stress factors and its prevalence among various bacteria underscore the importance of this RNA in regulation. While the mechanism of action of *micF* RNA is unclear, the RNA binds stably to the 5′-end of *ompF* mRNA *in vitro* (Andersen & Delihas, 1990) and participates in the destabilization of the *ompF* message *in vivo* (Andersen et al., 1989).

In this study, partial digestion by structure-specific ribonucleases (RNases)[1] and chemical modification by nickel complex [2,12-dimethyl-2,7,11,17-tetraazabicyclo[11.3.1]-heptadeca-1(17),2,11,13,15-pentaene]nickel(II) perchlorate (NiCR) (Chen et al., 1991, 1992, 1993) were employed to model the secondary structures of *micF* RNA, *ompF*-213 mRNA (a 213 nucleotide 5′-end segment of *ompF* mRNA), and the *micF* RNA/*ompF*-213 mRNA duplex. Both *micF* RNA and *ompF* mRNA have single-stranded 5′-ends and contain stable hairpin structures. The derived RNA/RNA duplex structure reveals an interaction between short segments of the two RNAs. In addition, while the RNA/RNA duplex comprises an imperfectly hybridized region, the Shine−Dalgarno sequence and AUG start codon of the *ompF*

† This work was supported by NSF Grant DMB-8803122 to N.D. M.S. was partially supported by NIGMS Public Health Services Training Grant 5-T32-GM07964-11. P.Z. was supported by NIH Grant GM 47531 to S. Rokita and C. Burrows.

* To whom correspondence should be addressed.

‡ Graduate Program in Genetics and Department of Molecular Genetics and Microbiology.

§ Department of Chemistry.

⊗ Abstract published in *Advance ACS Abstracts,* March 1, 1995.

[1] Abbreviations: RNase, ribonuclease; PCR, polymerase chain reaction; Tris, tris(hydroxymethyl)aminomethane; DTT, dithiothreitol; EDTA, ethylenediaminetetraacetic acid; TBE, 50 mM Tris-borate (pH 8.3) and 1 mM EDTA; SDS, sodium dodecyl sulfate; TMK buffer, 50 mM Tris-HCl (pH 7.5), 5 mM $MgCl_2$, and 25 mM KCl; NiCR, [2,-12-dimethyl-2,7,11,17-tetraazabicyclo[11.3.1]heptadeca-1(17),2,11,13,-15-pentaene]nickel(II) perchlorate.

0006-2960/95/0434-3621$09.00/0

message are base-paired to *micF* RNA. *micF* sequences from bacteria related to *E. coli* were compared, and the results show that the proposed secondary structure for *micF* RNA is phylogenetically conserved.

MATERIALS AND METHODS

Enzymes, Reagents, and Construction of Plasmid pUCT7-micF. Restriction enzymes, T4 polynucleotide kinase, calf intestinal alkaline phosphatase, and nucleotides were obtained from both Promega and Boehringer Mannheim. T4 RNA ligase was obtained from New England Biolabs. All RNases were obtained from Pharmacia LKB Biotechnology. NiCR was synthesized according to published procedures (Karn & Busch, 1966). Acrylamide and other chemicals were purchased from Sigma or Fisher. [γ-^{32}P]ATP was obtained from either NEN Research Products or ICN. [5′-^{32}P]pCp was obtained from NEN Research Products.

The *micF* gene was cloned upstream of a T7 promoter using the polymerase chain reaction (PCR) and conventional cloning techniques (Sambrook et al., 1989). The plasmid pKI0041 (Andersen et al., 1989), which contains the *micF* gene, was used as a template for the PCR reaction. PCR was performed using the GeneAmp Kit (Perkin Elmer) according to the instructions supplied by the manufacturer. The primers used were described previously (Andersen & Delihas, 1990). The PCR product was electrophoresed on a 1% agarose gel, excised from the gel, and recovered by electroelution. The fragment was further purified by phenol/chloroform extraction and ethanol precipitation.

The purified PCR-generated DNA was cloned into the *Hin*dIII and *Eco*RI sites in the multiple cloning region of plasmid pUC19 (Yanisch-Perron et al., 1985). The resulting plasmid, pUCT7micF, allows runoff *in vitro* transcription of *micF* RNA after plasmid DNA has been digested with restriction enzyme *Dra*I.

In Vitro Transcription with T7 RNA Polymerase. To synthesize *ompF*-213 mRNA, plasmid pJAN011 (Andersen & Delihas, 1990) DNA was digested with *Bgl*II restriction endonuclease; for *micF* RNA, plasmid pUCT7micF (see above) DNA was digested with *Dra*I restriction endonuclease. The digestions were phenol/chloroform extracted twice and ethanol precipitated. *In vitro* transcription was performed for 3 h at 37 °C using digested template DNA, at a concentration of 50 nM for pJAN011 and 125 nM for pUCT7micF, in a mixture containing 40 mM tris(hydroxymethyl)aminomethane (Tris)-HCl (pH 8.1), 20 mM $MgCl_2$, 1 mM spermidine, 5 mM dithiothreitol (DTT), 0.01% (v/v) Triton X-100, 4 mM each of ATP, CTP, GTP, and UTP, and 135 ng (40 units)/μL T7 RNA polymerase, which had been purified essentially as described previously (Grodberg & Dunn, 1988). The reaction volumes were 50μL.

Transcription was terminated by the addition of 0.1 vol of 3 M KOAc, pH 7.5, and 2.25 vol of 95% ethanol. The precipitated RNA was denatured by heating at 50 °C for 5 min in denaturing loading buffer [7 M urea, 5 mM Tris-borate (pH 8.3) and 1 mM ethylenediaminetetraacetic acid (EDTA)] and purified by gel electrophoresis on a 12% polyacrylamide gel containing 7 M urea in [50 mM Tris-borate (pH 8.3) and 1 mM EDTA (TBE)]. The RNA bands were visualized by UV shadowing and excised from the gel, and the RNA was eluted from the gel by vigorous shaking at 37 °C overnight in 400 μL of elution buffer [0.5 M NH_4-OAc (pH 7.5), 10 mM $Mg(OAc)_2$, 0.1% sodium dodecyl sulfate (SDS), and 1 mM EDTA]. The eluted RNAs were then ethanol precipitated, dried, and redissolved in sterile double-deionized water.

^{32}P End Labeling of RNAs. RNA was either 5′ labeled with [γ-^{32}P]ATP using polynucleotide kinase following treatment with alkaline phosphatase (Donis-Keller et al., 1977) or 3′ labeled with [5′-^{32}P]pCp using T4 RNA ligase (England & Uhlenbeck, 1978). Labeled RNA was isolated by electrophoresis on a 12% polyacrylamide gel containing 7 M urea in TBE. Labeled RNA was excised from the gel using an autoradiogram as a template, and the RNA was eluted by shaking the gel slice vigorously overnight at 37 °C in 400 μL of elution buffer containing 10 μg of carrier RNA (purified 5S RNA from wheat germ). The labeled RNA was subsequently ethanol precipitated, dried, and resuspended in double deionized water.

Renaturation of ompF-213 mRNA and micF RNA and Formation of the RNA/RNA Duplex. ^{32}P-end-labeled RNAs were renatured by heating to 55 °C for 5 min in TMK buffer [50 mM Tris-HCl (pH 7.5), 5 mM $MgCl_2$, and 25 mM KCl]. The RNA was then allowed to cool slowly (about 1 °C/min) to room temperature before being placed on ice. An alternative renaturation method was also used: RNAs were incubated in TMK buffer for 30 min at 37 °C and subsequently placed on ice. For the nickel reactions, labeled RNA was renatured in either 10 mM Tris-HCl (pH 7.5) and 0.5 mM $MgCl_2$ or 10 mM Tris-HCl (pH 7.0), 5 mM $MgCl_2$, and 25 mM KCl (the nickel reagent is sensitive to the presence of Mg^{2+} at pH 7.5 and more tolerant of this ion at pH 7.0). To form the RNA/RNA duplex, ^{32}P-end-labeled *ompF*-213 mRNA or *micF* RNA was renatured in the presence of a 5−10-fold molar excess of unlabeled RNA of the opposite type. Under these conditions, greater than 95% of the ^{32}P-end-labeled species was found in the duplexed form.

Partial Ribonuclease Digestions and Reaction with Nickel Complex. Renatured RNAs were treated with increasing amounts of RNase T2 (0.8−100 milliunits/μg of RNA), RNase T1 (1−200 milliunits/μg of RNA), or RNase V1 (0.07−10 milliunits/μg of RNA) in the presence of 10 μg of unlabeled carrier 5S RNA. In the case of digestion by RNase V1, NaCl and additional $MgCl_2$ were added to a final concentration of 175 and 10 mM, respectively, to ensure proper enzymatic function. The digestions were performed at 23 °C, for either 5−30 min (RNase T1), 30 min (RNase T2), or 15 min (RNase V1), and the reaction volumes were 10 μL. The digestions were terminated by the addition of 10 μL of 40 mM EDTA and were placed on ice. Each reaction was phenol/chloroform extracted, ethanol precipitated, dried, and resuspended in denaturing loading buffer.

Renatured RNAs were incubated with NiCR (30 μM) and $KHSO_5$ (200 μM) in the presence of 2 μg of unlabeled carrier 5S RNA. The incubations were performed at 23 °C for 30 min, and the reaction volumes were 20 μL. The reactions were terminated by the addition of 180 μL of stop solution [10 mM Tris-HCl (pH 7.5), 0.3 M NaOAc, 10 mM EDTA (pH 8.0), and 0.5% SDS] containing 3 μg of 5S RNA. Each reaction was phenol/chloroform extracted, ethanol precipitated, dried, and incubated with 20 μL of 1 M aniline acetate (pH 4.6) at 60 °C for 20 min; the samples were then lyophilized and washed with water.

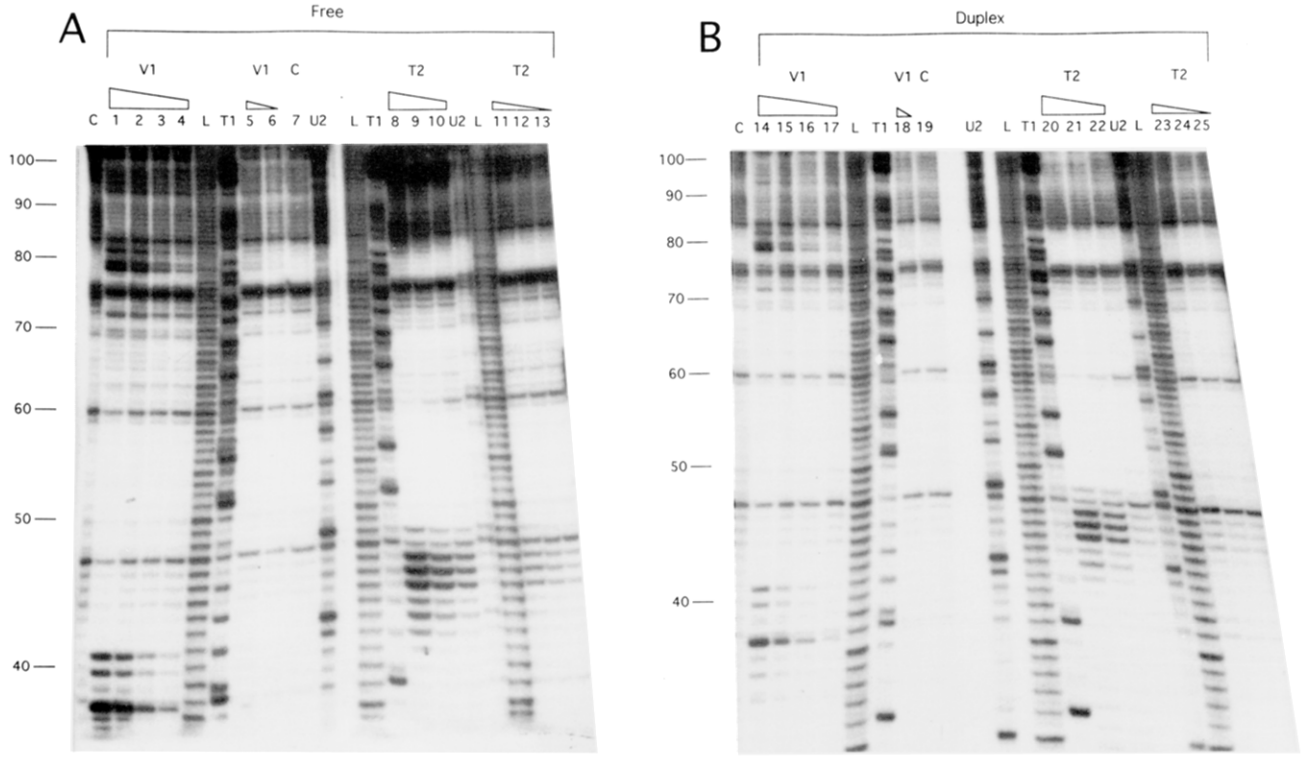

FIGURE 1: Sequencing gels showing the cleavage pattern of *ompF*-213 mRNA after partial digestion with RNases V1 and T2, positions 45−105. (A) Free *ompF*-213 mRNA. 5′-labeled sample on 12% polyacrylamide gel: lanes 1−6 are digestions with RNase V1 at concentrations of 2, 1, 0.6, 0.3, 0.1, and 0.07 milliunits/μg RNA, respectively; lane 7 is a nondigested, renatured control sample; lanes 8−13 are digestions with RNase T2 at concentrations of 20, 10, 6, 3, 2, and 0.8 milliunits/μg RNA, respectively. Sequencing lanes marked T1 and U2 are partial digestions with RNases T1 and U2, respectively, under denaturing conditions; the lane marked L is an alkaline hydrolysis ladder; the lane marked C (far left) is undigested control under denaturing conditions. (B) *ompF*-213 mRNA in the RNA/RNA duplex. 5′-labeled sample on 12% polyacrylamide gel: lanes 14−18 are digestions with RNase V1 at concentrations of 2, 1, 0.6, 0.3, and 0.1 milliunits/μg RNA, respectively; lane 19 is a nondigested, renatured control sample; lanes 20−25 are digestions with RNase T2 at concentrations of 20, 10, 6, 3, 2, and 0.8 milliunits/μg RNA, respectively. Lanes marked T1, U2, L, and C (far left) are as described for panel A. Gels A and B were run at the same time with the same RNA batch; two gels were used because of the large number of samples.

Gel Electrophoresis and Analysis of Cleavage Products. The digested RNA was heated at 50 °C for 5 min to ensure denaturation and loaded onto a sequencing gel containing 6, 8, or 12% polyacrylamide, 7 M urea, and TBE. Gel electrophoresis was performed at 1500−2000 V until marker dyes reached predetermined positions. The gels were subsequently autoradiographed at −70 °C on Fuji X-ray film using an intensifier screen if necessary.

Cleavage positions were assigned by comparison of cleavage products to enzymatic RNA sequencing lanes and an alkaline hydrolysis ladder. End-labeled RNAs were subjected to partial digestion by RNase T1 (which cleaves after G residues) or RNase U2 (which cleaves after A residues) at 55 °C for 12 min in the presence of 7 M urea at pH 5 (RNase T1) or pH 3.5 (RNase U2) to obtain sequencing lanes. Alkaline hydrolysis ladders were generated by incubating end-labeled RNA at 90 °C for 5 min at pH 9.4. Band intensities were determined by visual inspection of autoradiograms.

Cleavage of RNA with RNase V1 results in fragments containing 5′-phosphates whereas alkaline hydrolysis and cleavage by RNases T1 and T2 yield fragments with 3′-phosphates. Assignment of RNase V1 cleavage positions on polyacrylamide gel patterns were made on the basis of differences between charge and mass of the resulting V1 digestion fragments and those generated by alkaline hydrolysis (Auron et al., 1982).

Computer Modeling. Computer modeling was performed utilizing the mfold package (Zuker, 1989; Jaeger et al., 1989, 1990; Zuker, 1994) with energy rules developed by Turner and colleagues (Freier et al., 1986; Turner et al., 1987, 1988). We used the "N best" mode with $p = 10\%$ except in the case of *micF* RNA, where we used $p = 20\%$ due to its small size.

Phylogenetic Comparison of Heterologous micF Sequences. Alignment of heterologous sequences and interpretation of phylogenetic data was performed according to previously published guidelines (Pace et al., 1989). Homology values were determined according to Sogin et al. (1986) using the formula $H = m/(m + u + g/2)$, where m refers to matching nucleotides, u to unmatching nucleotides, and g to gaps in the nucleotide sequence.

RESULTS

Secondary Structural Probe of the 5′-End of ompF mRNA. *ompF*-213 mRNA was synthesized and radioactively end-labeled *in vitro*, purified by polyacrylamide gel electrophoresis, renatured, and probed by partial nuclease digestion with RNase T2, RNase T1, and RNase V1 (Ehresmann et al., 1987). RNase T2 recognizes and cleaves single-stranded regions of an RNA with little sequence specificity, while RNase T1 cleaves after single-stranded G residues. RNase V1 recognizes helically oriented nucleotides, whether they are base-paired or not (Lowman & Draper, 1986). Because nuclease probes are sensitive to steric hindrance, chemical

modifications were performed using the NiCR reagent to gain additional information. This and other nickel complexes have been shown to be useful in probing the structures of RNA and DNA (Chen et al., 1991, 1992, 1993), as their reaction correlates to the solvent exposure of the N7 position of guanine residues. We also note the positions of basal cleavages, which occur in the absence of added nucleases and may be due to self-cleavage in single-stranded regions (see Discussion). Representative autoradiograms of polyacrylamide gel separations of nuclease digestion and NiCR modification products are shown in Figures 1A and 2A. The nuclease cleavage and nickel modification sites are graphically displayed on a modified computer-generated secondary structural model obtained using the method of Zuker (1994) (Figure 3). Computer-predicted pairings not supported by the probing data (Figures 1A and 2A) are not depicted in Figure 3. The cleavage sites shown in Figure 3 represent a consensus of three or more probing determinations.

Nuclease and chemical modification probing data are consistent with one of the suboptimal computer generated secondary structural models for *ompF*-213 mRNA consisting of two major and one minor stem loop structures (Figure 3). Given the regulatory antisense nature of *micF* RNA, the structure encompassing the region which contains the ribosome-binding site and AUG start codon is particularly important. Strong RNase T1 and T2 cleavages were obtained in the proposed loop of helix IA, along with nickel modification at position G97, consistent with the existence of this stem-loop, although no RNase V1 cleavages were obtained in the stem of this helix. Since RNase V1 needs a stretch of at least four nucleotides to recognize a helix (Lowman & Draper, 1986), V1 cleavages would not be expected to occur in helix IA. Moderate cleavages by RNase T1 are sometimes observed at positions 99, 100, and 101, along with nickel modifications; this may indicate that helix IA is unstable or that subpopulations of molecules exist, some containing helix IA and some more loosely structured in this region. In any event, the ribosome binding site GAGG100 (underlined, Figure 3) and the AUG113 initiation codon (indicated in Figure 3) appear to be accessible to single-strand-specific nucleases, and the presence of T2, T1, and basal cleavages supports the single-stranded character of positions 83−91 and 103−126. Additionally, guanine residues 113, 116, 119, and 121 are all reactive with NiCR.

Helix I is defined by the following cleavages. There are 10 RNase V1 sites on the 5′ side of helix I starting at position 14, one at position 71, and three on the 3′ side of the base of this helix, at positions 78, 79, and 81. All guanine residues proposed to be in double-stranded regions of helix I do not react with NiCR, as expected. Strong RNase T2 cleavages were obtained in the proposed loop of helix I at positions 44−46. Additional RNase T2 cleavages seen at positions 41−43 indicate that either this loop encompasses positions 42−49 or that there is extensive breathing at the A-U base pairs that close the loop. The internal loop close to the base of helix I is partially defined by RNase T2 and/or T1 cleavages at positions 73 and 74; G74 is also the site of a strong nickel modification. The fact that G73 is only weakly modified by the nickel reagent implies that it may be able to pair with A19, making its N7 position less accessible. Continuous RNase V1 cleavages occur from positions U34 to A40. Since RNase V1 will cleave at a stacked base whether it is base-paired or not (Lowman & Draper, 1986),

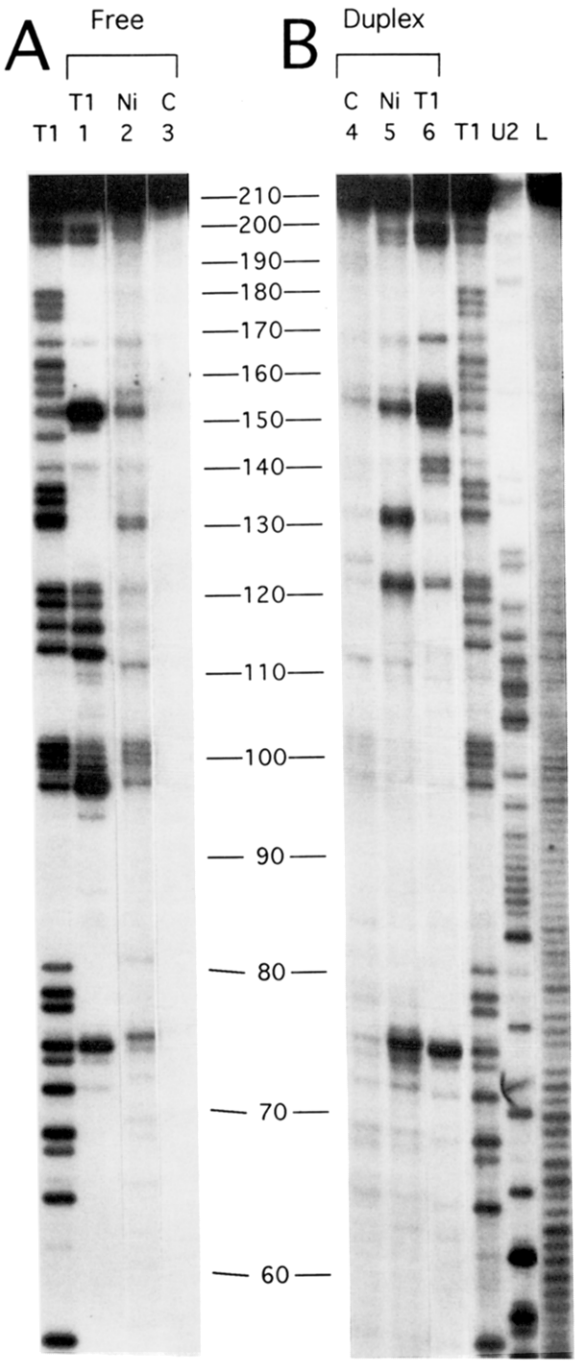

FIGURE 2: Sequencing gels showing the cleavage pattern of *ompF*-213 mRNA after partial digestion with RNase T1 or chemical modification with NiCR, positions 53−213. (A) Free *ompF*-213 mRNA. 5′-labeled sample on 8% polyacrylamide gel: lane 1 is a digestion with RNase T1 (5 milliunits/μg RNA); lane 2 is a chemical modification with NiCR (30 μM) followed by aniline treatment; lane 3 is a nondigested, renatured control sample. (B) *ompF*-213 mRNA in the RNA/RNA duplex. 5′-labeled sample on 8% polyacrylamide gel: lane 4 is a nondigested, renatured control sample; lane 5 is a chemical modification with NiCR (30 μM) followed by aniline treatment; lane 6 is a digestion with RNase T1 (5 milliunits/μg RNA). Sequencing lanes marked T1 and U2 are partial digestions with RNases T1 and U2, respectively, under denaturing conditions; the lane marked L is an alkaline hydrolysis ladder.

the observed cleavages imply that the bulged positions C37 and A40 are stacked within the helix (the same reasoning may also apply to position C23). While either nucleotides U59 or U60 could be paired with A32, the presence of a basal cleavage at U60 implies that it is the unpaired

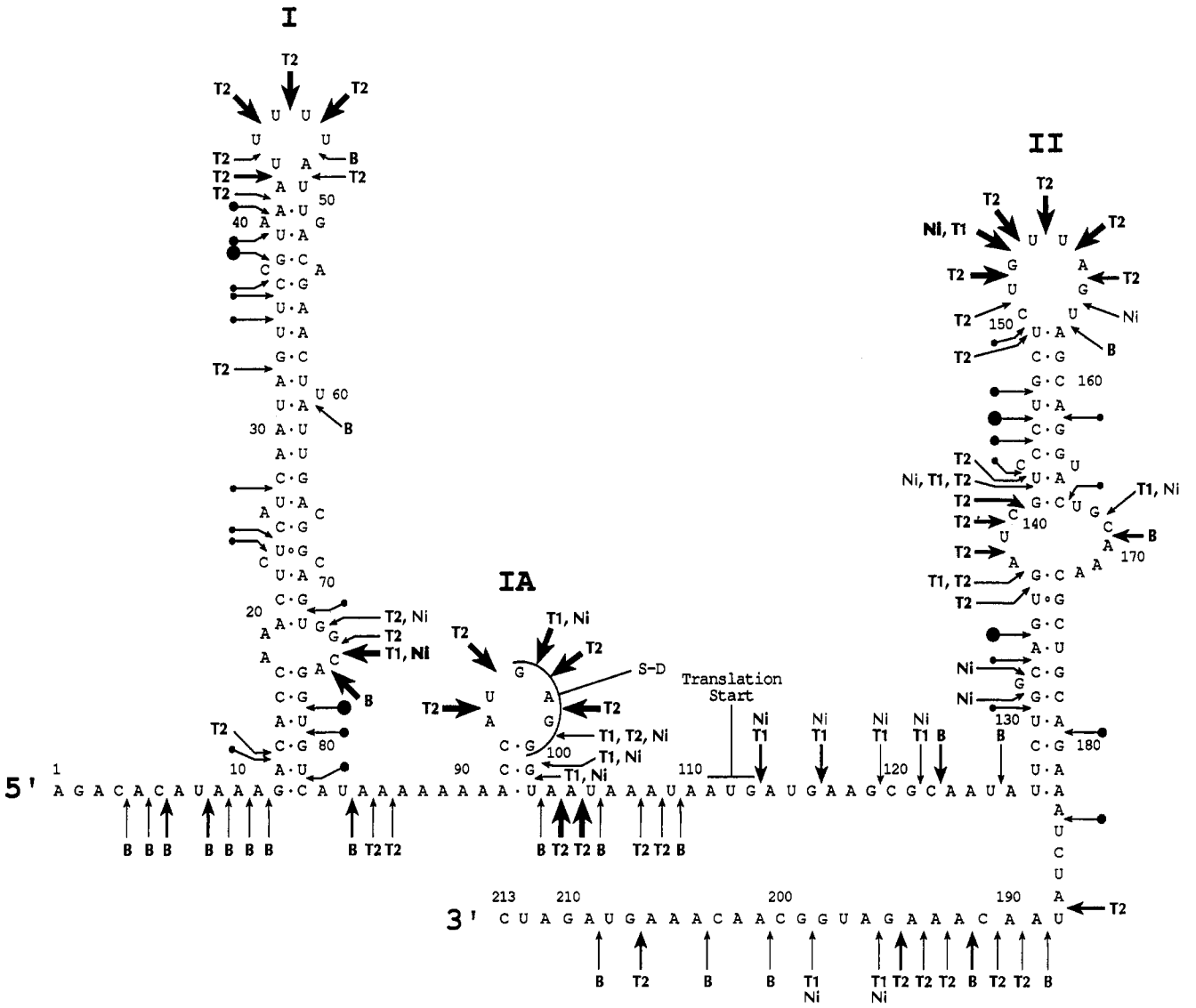

FIGURE 3: Proposed secondary structure for *ompF*-213 mRNA. Arrows mark the primary ribonuclease cleavage and chemical modification sites. The following symbols at the end of arrows represent the respective ribonuclease: T1, RNase T1; T2, RNase T2; ●, RNase V1. The symbol Ni at the end of an arrow represents a nickel complex modification. The symbol B at the end of an arrow represents a basal cleavage (see text). In the case of arrows representing T1, T2, and B cleavages, the boldness of the arrow corresponds to the intensity of the cleavage; in the case of arrows representing V1 cleavages, the size of the circle corresponds to the intensity of the cleavage; in the case of arrows representing nickel complex modifications, the boldness of the symbol Ni corresponds to the intensity of the modification. The symbol S-D indicates the Shine–Dalgarno sequence. The AUG translation start codon is also indicated.

nucleotide in this region; another interpretation would be that both pairings exist in equilibrium, and cleavage is more likely when U60 is unpaired due to its U/A context.

With the exception of the basal cleavages, no significant enzymatic cleavages were obtained in the 5′ tail region comprising positions 1−11. The presence of these basal cleavages, however, is consistent with the predicted single-stranded character of this region.

The nuclease digestion and chemical modification patterns in helix II are consistent with the model for this stem-loop shown in Figure 3. The remainder of the molecule, 3′ to helix II, exhibits strong cleavages by RNases T1 and T2, as well as nickel modifications at positions G195 and G198, indicating that this region appears to be single-stranded.

Secondary Structural Probe of micF RNA. *micF* RNA was synthesized and end-labeled *in vitro*, purified by gel electrophoresis, renatured, and probed with ribonucleases. A representative autoradiogram is shown in Figure 4A. In Figure 5 the nuclease cleavage sites are superimposed on a computer-generated secondary structural model obtained using the method of Zuker (1994) for *micF* RNA. Partial nuclease cleavage data are highly consistent with this secondary structural model, which predicts two stem-loop structures and a long, single-stranded 27-nucleotide sequence at the 5′-end. V1 cleavages from positions 30−34 and at position 44, along with T2 cleavages at positions 37−39, define stem-loop I. The RNase V1 cleavages at positions U49 and G50 support the inclusion of base pairs C-G(28/50) and G-U(29/49) in this helix. In addition, the RNase V1 cleavages at the base of stem I at positions U47 and C48 and at position U30 suggest that these bases are stacked. The V1 cleavage at U51 (a position found outside the stem) may indicate that this position is also stacked. Stem II, which is followed by six unpaired uridine residues, forms a classic Rho-independent transcriptional termination structure. V1 cleavages at positions 68, 69, 71, 81, 83, and 84, along with T2 cleavages at positions 75 and 88−92, support the existence of this predicted structure. The proposed single-

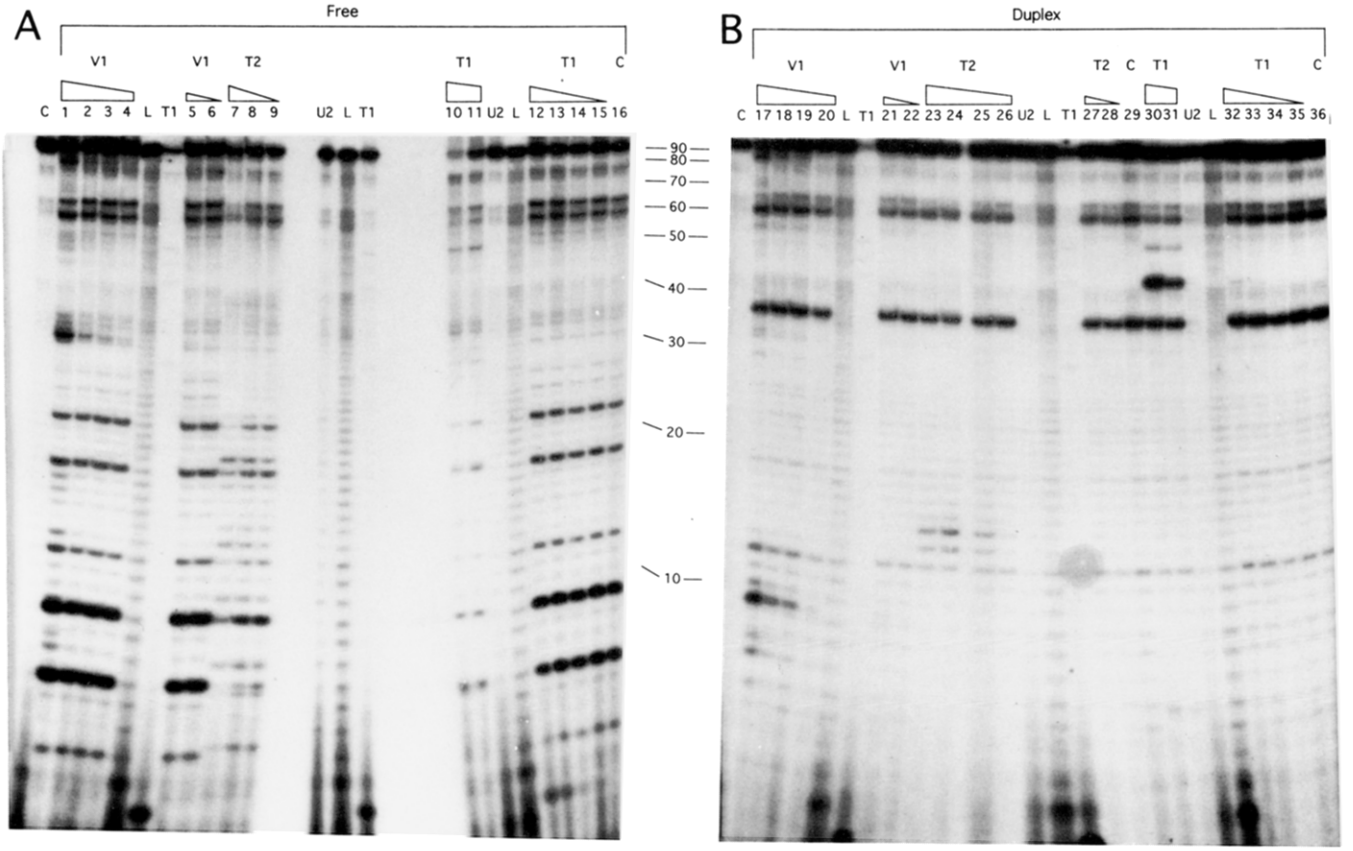

FIGURE 4: Sequencing gels showing the cleavage pattern of *micF* RNA after partial digestion with RNases V1, T2, and T1. (A) Free *micF* RNA. 5′-labeled sample on 12% polyacrylamide gel: lanes 1−6 are digestions with RNase V1 at concentrations of 10, 5, 2, 1, 0.6, and 0.3 milliunits/μg RNA, respectively; lanes 7−9 are digestions with RNase T2 at concentrations of 100, 50, and 20 milliunits/μg RNA, respectively; lanes 10−15 are digestions with RNase T1 at concentrations of 200, 100, 10, 5, 2, and 1 milliunits/μg of RNA, respectively; lane 16 is a nondigested, renatured control sample. Sequencing lanes marked T1 and U2 are partial digestions with RNases T1 and U2, respectively, under denaturing conditions; the lane marked L is an alkaline hydrolysis ladder; the lane marked C (far left) is undigested control under denaturing conditions. (B) *micF* RNA in the RNA/RNA duplex. 5′-labeled sample on 12% polyacrylamide gel: lanes 17−22 are digestions with RNase V1 at concentrations of 10, 5, 2, 1, 0.6, and 0.3 milliunits/μg RNA, respectively; lanes 23−28 are digestions with RNase T2 at concentrations of 100, 50, 20, 10, 6, and 3 milliunits/μg RNA, respectively; lanes 30−35 are digestions with RNase T1 at concentrations of 200, 100, 10, 5, 2, and 1 milliunits/μg of RNA, respectively; lanes 29 and 36 are nondigested, renatured control samples. Lanes marked T1, U2, L, and C (far left) are as described for panel A. Gels A and B were run at the same time with the same RNA batch; two gels were used because of the large number of samples.

stranded character of positions 1−27 and 52−64 is supported by the presence of T2 and basal cleavages in these regions. The current *micF* RNA structural model is consistent with a theoretical model presented previously for *micF* RNA (Andersen et al., 1987), but there are minor exceptions. Notably, the previous model showed helix I ending with the base pair C-G (positions 31/46) whereas in the current model this helix extends to a C-G pair at positions 28/51.

ompF-213 mRNA/micF RNA Duplex Structure. To determine the secondary structure of the RNA/RNA duplex, probing was carried out in two ways. Either ^{32}P-end-labeled *ompF*-213 mRNA was incubated with a 10-fold molar excess of unlabeled *micF* RNA or ^{32}P-end-labeled *micF* RNA was incubated with an excess of unlabeled *ompF*-213 mRNA. Under these conditions, greater than 95% of the labeled species was found in the duplexed form. Incubation mixtures were partially digested with ribonucleases or subjected to NiCR modification and electrophoresed on denaturing polyacrylamide gels (see Figures 1B and 2B for analysis of *ompF*-213 mRNA and Figure 4B for analysis of *micF* RNA). In addition, some duplex probing experiments were done in the following fashion: the RNA/RNA hybrid was formed and digested as above, but then the digested material was separated on a nondenaturing polyacrylamide gel, the band representing the duplex was excised and eluted, and this RNA was analyzed on a sequencing gel. Results did not differ depending upon which method was used. Figure 6 shows the proposed model for the *ompF*-213 mRNA/*micF* RNA interaction along with the nuclease cleavage and nickel modification sites. The model is a modified computer-generated secondary structure obtained using the method of Zuker (1994). Predicted pairings not supported by the data are not depicted.

A comparison of probing data from free and duplexed *ompF*-213 mRNA reveals a nearly identical pattern of nuclease cleavages and NiCR modifications in the 5′-end of the RNA up to position A82. The pattern of both nuclease digestion and chemical modification markedly differs, however, in the segment proposed to interact with *micF* RNA, positions A95−C120 (compare Figures 3 and 6). The strong RNase T2 and T1 cleavages at positions 95−99, 103, and 104, and other T1 and T2 cleavages at positions 107, 108, 113, 116, 119, and 121 in free *ompF*-213 mRNA are not present in the duplexed message (Figures 1 and 2). Instead, RNase V1 cleavage occurs at positions G101−A104. Additionally, all guanine residues in this region (97, 99−101,

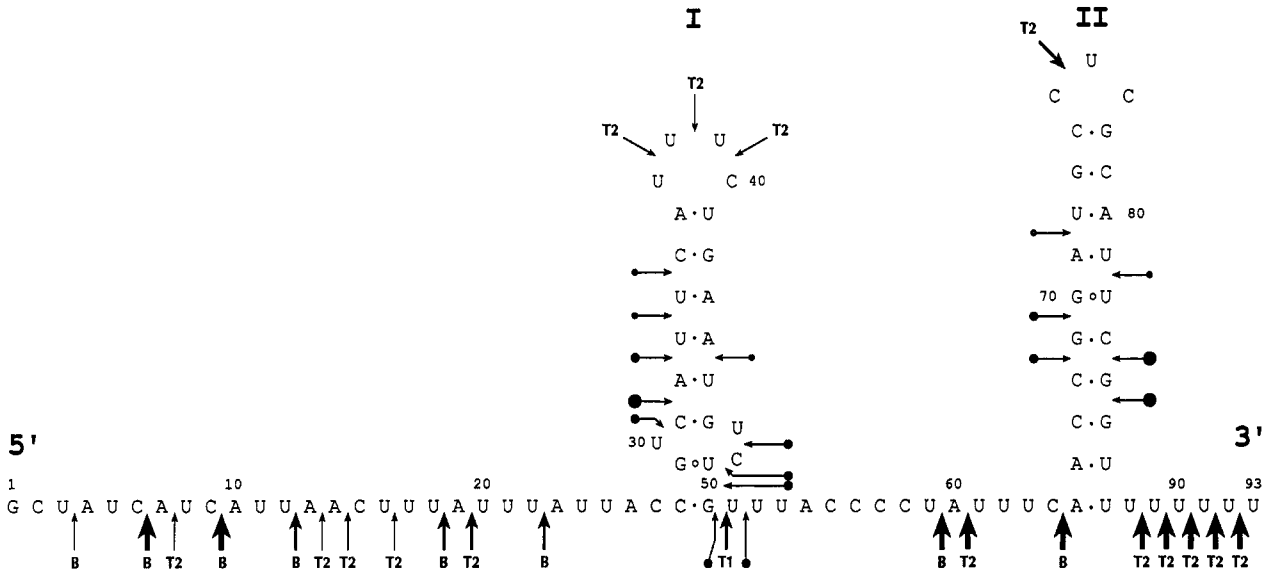

FIGURE 5: Proposed secondary structure for *micF* RNA. Arrows mark the primary ribonuclease cleavage sites. The following symbols at the end of arrows represent the respective ribonuclease: T1, RNase T1; T2, RNase T2; ●, RNase V1. The symbol B at the end of an arrow represents a basal cleavage (see text). In the case of arrows representing T1, T2, and B cleavages, the boldness of the arrow corresponds to the intensity of the cleavage; in the case of arrows representing V1 cleavages, the size of the circle corresponds to the intensity of the cleavage.

113, 116, and 119), which are reactive with NiCR when *ompF*-213 mRNA is in its free form, become unreactive in the duplexed form, indicating base pairing with *micF* RNA in this region. The assignment of bulged positions G99 and A108 of *ompF* mRNA as opposed to adjacent nucleotides is arbitrary, since alternate pairings are acceptable. The 3′ region of the RNA from positions 121−213 shows nearly the same nuclease cleavages and NiCR modifications in free and duplexed *ompF* mRNA. Thus, helices I and II and positions adjacent to them do not show significant alteration in partial digestion patterns from free and duplexed forms and are probably not involved in the interaction with *micF* RNA.

A comparison of nuclease probe data of free and duplexed *micF* RNA shows that the 5′-end up to position 50 shows a markedly different partial nuclease digestion pattern (compare Figures 5 and 6). There is no evidence for the presence of stem loop I of *micF* RNA in the proposed duplex structure, and the RNase T2 cleavages in the 5′ single-stranded region of free *micF* RNA are absent in duplexed *micF* RNA. In addition, duplexed *micF* RNA has a very strong basal cleavage at position C35 that is not present in free *micF* RNA, and RNase V1 cleavage sites at positions 7, 9−11, and 29 are found only in duplexed *micF* RNA (Figure 4). These V1 cleavage sites support the proposed base pairing shown in Figure 6, and the RNase T2 cleavages at positions 13 and 14 are consistent with the proposed looped-out region of duplexed *micF* RNA. Bulged positions A4 and G29 of *micF* RNA show no nuclease susceptibility, but their assignment as bulged nucleotides maintains the continuity of adjacent base pairs.

The RNase T1 cleavages at positions 42, 46, and 50 of *micF* RNA in the duplexed form suggest that this region is single-stranded; however, the region comprising positions U34−C58 appears to be relatively opaque to RNase T2. In addition, the lack of RNase V1 cleavages is consistent with the proposed single-stranded character of this region. The pattern of RNase cleavages in stem loop II and adjacent single-stranded sequences of free and duplexed *micF* RNA are almost identical, and thus this region does not appear to interact with *ompF*-213 mRNA. The sum total of the nuclease probing results of duplexed *micF* RNA/*ompF*-213 mRNA indicates a high consistency with the proposed model predicting the interaction of the segment 1−33 of *micF* RNA with the segment 95−120 of *ompF* mRNA.

All of the data shown are from partial nuclease digestion experiments utilizing RNA labeled at its 5′-end; however, probing was also carried out using 3′-labeled RNA (data not shown). Data from experiments using 3′-labeled RNA were in agreement with that obtained utilizing 5′-labeled material.

DISCUSSION

On the basis of experimental probing data and computer analyses, we propose secondary structural models for *micF* RNA, the 5′-end of the target *ompF* mRNA, and the RNA/RNA duplex. The structure-specific nuclease cleavage sites in free *micF* RNA appear to be in good agreement with the domains predicted by the computer folding program to be single-stranded and double-stranded (Figure 5). The nuclease cleavage sites in the regions forming the RNA/RNA duplex, positions 1−33 of *micF* RNA and 95−120 of *ompF* mRNA, along with NiCR modification data are entirely consistent with the optimal computer-predicted structure (Figure 6). The majority of nuclease cleavages and NiCR modifications support the model for *ompF*-213 mRNA, although there are exceptions. For example, there are RNase T2 cleavages of moderate intensity at proposed stem I of *ompF* mRNA at positions 13, 32, and 41−43 (Figure 3). The cleavage at A13 may represent breathing at the base of the stem. RNase T2 cleavages at positions 41−43 may indicate either breathing at the loop closure or that the loop encompasses eight nucleotides. The RNase T2 cleavage at A32 may indicate breathing in this area or the presence of a minor alternate conformer. This region of helix I consists predominantly of A-U base pairs and has a bulged nucleotide at position 60. In helix II, the presence of T1 and/or T2 cleavages at positions 136, 137, 141, and 142, along with minor nickel

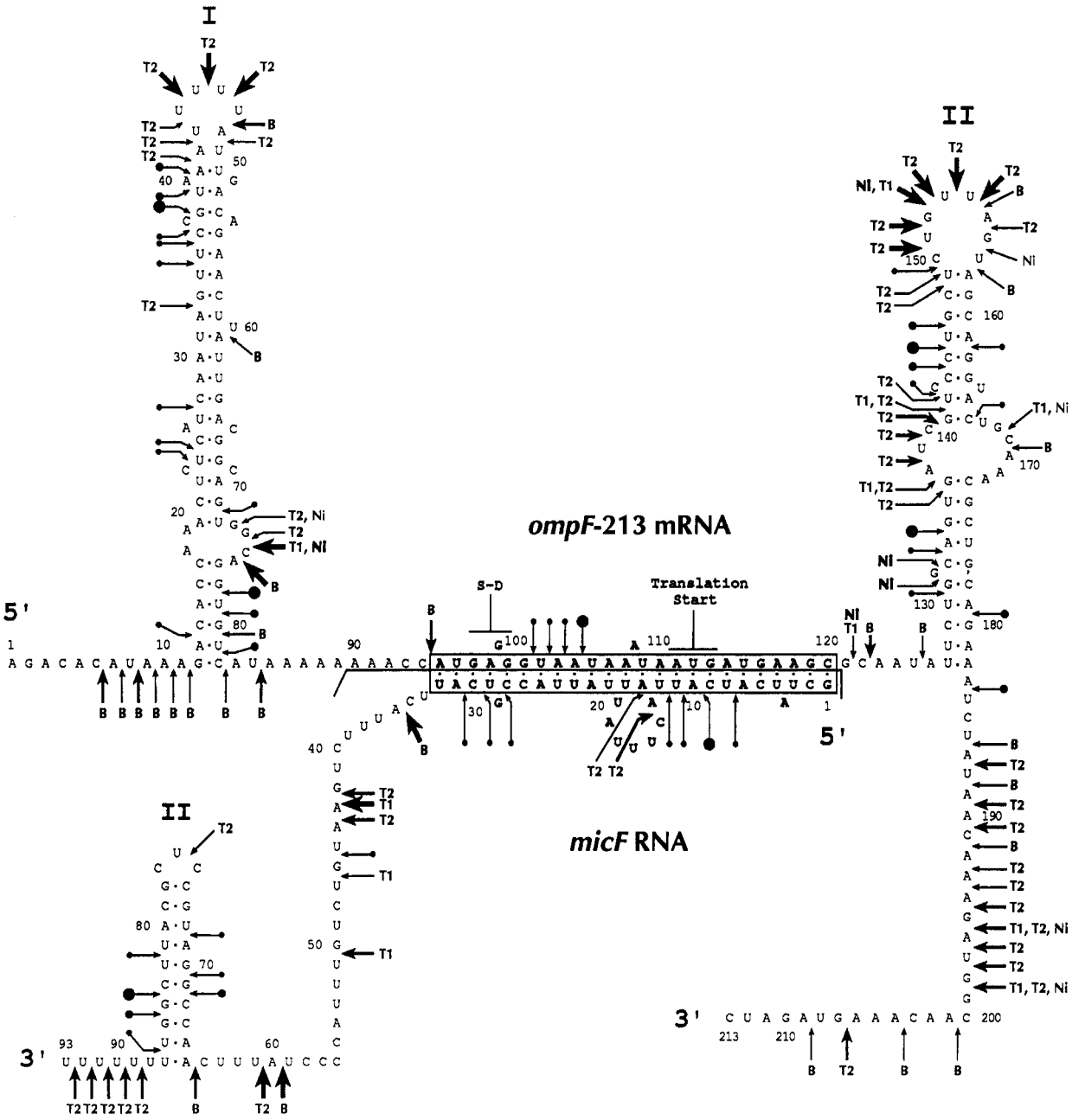

FIGURE 6: Proposed secondary structure for the *ompF*-213 mRNA/*micF* RNA duplex. Arrows mark the primary ribonuclease cleavage and chemical modification sites. The following symbols at the end of arrows represent the respective ribonuclease: T1, RNase T1; T2, RNase T2; ●, RNase V1. The symbol Ni at the end of an arrow represents a nickel complex modification. The symbol B at the end of an arrow represents a basal cleavage (see text). In the case of arrows representing T1, T2, and B cleavages, the boldness of the arrow corresponds to the intensity of the cleavage; in the case of arrows representing V1 cleavages, the size of the circle corresponds to the intensity of the cleavage; in the case of arrows representing nickel complex modifications, the boldness of the symbol Ni corresponds to the intensity of the modification. The symbol S-D indicates the Shine–Dalgarno sequence. The AUG translation initiation codon is also indicated.

modification at G141, shows that breathing probably occurs at the closure of the internal loop on this side of the helix, possibly due to the asymmetry of this internal loop.

It is of interest that the optimal and several suboptimal computer-generated secondary structures for the *micF* RNA/*ompF*-213 mRNA duplex predict base pairing between positions 1–5 of *ompF*-213 mRNA and positions 49–45 of *micF* RNA. This pairing is not included in our proposed structure due to incomplete support from the probing data (see Figure 6). An RNase T1 cleavage occurs at position G47, while an RNase V1 cleavage site exists at position 46. Additionally, basal cleavages at positions 4 and 5 in free *ompF*-213 mRNA seem to disappear in the duplexed form. These results may indicate a weakly stable pairing of the RNAs in these regions such that both forms are present under our probing conditions.

The data obtained with NiCR are consistent with the nuclease cleavage data; because of the small size of the nickel reagent, it can also provide insight into some aspects of the structures that the nucleases cannot because of their sensitivity to steric hindrance. In *ompF*-213 mRNA, for example, the fact that both G131 and G132 exhibit strong, equal reactivity with NiCR implies that either residue may be paired with C178. The reduced activity of the loop residue G156 with NiCR (compared with G152) implies that its N7 position is relatively inaccessible. A possible explanation

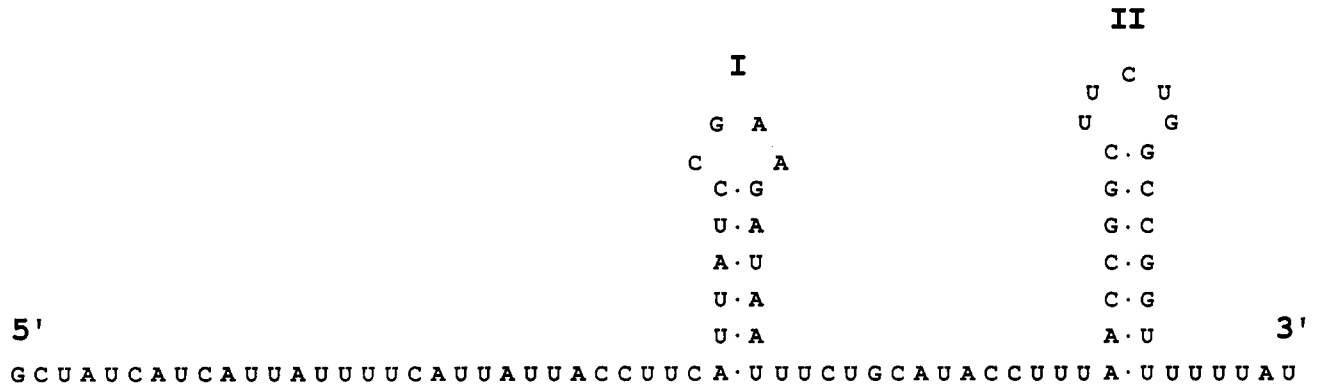

FIGURE 7: Proposed secondary structure for *S. marcescens micF* RNA. The model was constructed using computer modeling and visual inspection after performing a phylogenetic comparison of *micF* sequences from *E. coli* and *S. marcescens*. Nucleotide sequence according to Hutsul and Worobec (1994).

for this may be the existence of a hydrogen bond involving G156 and C150, leaving U157 bulged out.

In the RNA/RNA duplex, the lack of reaction with NiCR at any of the *ompF*-213 mRNA guanine residues 99−101 implies that the N7 positions of these nucleotides are inaccessible to the solvent and may mean that none of them are actually bulged out from the helix. One explanation for this observation could be the existence of a non-Watson−Crick base pair involving position G99 of *ompF*-213 mRNA and position G29 of *micF* RNA, with the two nucleotides stacked within the helix.

Basal cleavages (B) are shown in line drawing figures in the text; they appear in the absence of added ribonuclease during incubation of RNAs under conditions used for probing, predominantly in *micF* RNA (see lanes 16, 29, and 36, Figure 4). Similar cleavages have been observed by others in nuclease probing experiments [e.g., Romby et al. (1985)]. Such cleavages largely occur at Y/A sequence junctions in regions of an RNA that are not base-paired or stacked and are thought to represent self-cleavage (Dock-Bregeon & Moras, 1987). Although it is difficult to rule out trace ribonuclease contamination to explain the cleavages observed in this study, several experiments were carried out to test this possibility. Multiple controls using autoclaved and/or double-deionized water with different combinations and preparations of buffers were performed and the cleavages always appeared, and at the same positions. In addition, we found that added divalent magnesium ion is not required for hydrolysis, which helps to rule out cleavage by a ribonuclease. Basal cleavages are ancillary to the nuclease probing and chemical modification data but are listed because they are clearly visible on gels and aid in defining single-stranded regions of RNA.

Basal cleavages seen in *micF* and *ompF* RNAs are useful in analysis of secondary structures. For example, no basal cleavage is observed in free *micF* RNA at the C/A junction at positions 35/36 where these positions are found base-paired in helix I (Figure 5). A strong basal cleavage is observed at this same junction, however, when *micF* RNA is in the RNA/RNA duplex where helix I appears to be disrupted (Figure 6). The lack of a basal cleavage at position C94 of free *ompF*-213 mRNA, presumably because this nucleotide is stacked in helix IA, is another example. This basal cleavage is readily observable in the RNA/RNA duplex, where this position now finds itself in a single-stranded environment. Also, several basal cleavages at Y/A junctions are found in the 5′-end of free *micF* RNA. These basal cleavages are not seen in duplexed *micF* RNA (Figure 4).

An important method of corroborating secondary structure models derived from structure probing data involves the phylogenetic comparison of gene sequences from related species (Fox & Woese, 1975; Delihas et al., 1984; Pace et al., 1989). The *micF* gene and its transcript have been identified in several species of Gram-negative bacteria, and the sequences of heterologous *micF* genes are known (Esterling & Delihas, 1994; Hutsul & Woroboc, 1994). *micF* sequences from *Klebsiella pneumoniae* and two species of *Salmonella* are highly homologous to *E. coli micF*. Base changes in these heterologous sequences are seen only in the proposed loop nucleotides of hairpin structures and the oligouridine tail at the 3′ end of *E. coli micF* RNA. On the other hand, the *micF* sequence from *Serratia marcescens* has diverged appreciably from that of *E. coli* (only 66% similarity exists). Values of 60−80% are considered optimal for phylogenetic analyses of secondary structures (Pace et al., 1989). A putative helix is considered nominally proven when two or more independent nucleotide covariations occur such that their canonical base pairing potential is maintained (Pace et al., 1989). At least two such covariations occur in both proposed helices I and II of our *micF* RNA secondary structure model when the *E. coli* and *S. marcescens* sequences are aligned and analyzed, providing corroborating evidence for their existence.

With this in mind, using computer folding and visual inspection, we generated a secondary structural model for *S. marcescens micF* RNA (Figure 7). There are several interesting similarities and differences between the *E. coli* and *S. marcescens* models. Both models have in common the presence of helices I and II separated by a single-stranded region, and each contains a 5′-single-stranded sequence and a 3′-single-stranded tail. It is of major interest that the positions of the two helices relative to each other are conserved exactly; there are 14 nucleotides separating hairpins I and II in both species. This could be important in recognition of another factor (e.g., the *micF* RNA-binding protein) or the conservation of an RNase E cleavage site. A UAY sequence (at position 59−61 of *E. coli micF* RNA) is phylogenetically conserved between helices I and II in *S. marcescens*. This sequence is part of an RNase E cleavage site in *E. coli micF* RNA (Schmidt, Mackie, and Delihas,

unpublished data). Other interesting similarities between the models include the conservation of short sequences flanking the stem-loop structures. On the other hand, the loops of the helices contain different nucleotide sequences in both species, and the stems of both hairpins I and II are shorter in *S. marcescens;* this is due to the deletion of *S. marcescens* sequences, most notably the region corresponding to *E. coli micF* positions 46−51.

No heterologous *ompF* mRNAs have yet been sequenced, so this type of phylogenetic analysis cannot be performed with *ompF* mRNA or the RNA/RNA duplex. It is of importance to note, however, that the *micF* RNA nucleotide sequence corresponding to the proposed *micF* RNA/*ompF* RNA interaction region (positions 1−33 in *E. coli micF* RNA) exhibits a very high degree of homology between *E. coli* and *S. marcescens* compared with the rest of the *micF* sequence. This region is 87% homologous (actually, positions 1−13 are 100% conserved), while positions 34−93, which are not proposed to interact with *ompF* mRNA, show only 53% homology. In fact, there is a marked discontinuity of homology in sequences immediately following the proposed binding region (Figure 6); *micF* RNA positions 34−50, for example, show only 32% homology between *E. coli* and *S. marcescens*. While the *S. marcescens ompF* sequence is not known, the high level of homology in the region proposed to interact with *ompF* mRNA would lend indirect support to the duplex model, since regions of intermolecular RNA/RNA pairing may be more constrained than other regions.

A *micF* RNA/*ompF* mRNA duplex has not been found to form to a significant extent with incubation at 0 °C; the duplex forms at 37 °C (Andersen & Delihas, 1990). Formation of the duplex structure involves the interaction of the unstructured 27 nucleotides at the 5′-end and 6 nucleotides of stem I of *micF* RNA with the largely unstructured region of *ompF* mRNA consisting of positions 95−120 (compare Figures 3, 5, and 6). Therefore, it appears that only stem I of *micF* RNA and the minor stem IA of *ompF* mRNA need to unfold to allow formation of the duplex structure. The lack of duplex formation at 0 °C may predominantly reflect the need for helix I of *micF* RNA to unfold. Information of this nature may be important in the design of synthetic antisense RNAs; it appears in this case that the interactions between the two RNAs occur largely in initially unstructured regions.

The duplex model presented in Figure 6 shows a hybridized region essentially comprised of two turns of a helix. The duplex may form by initial interaction of the unstructured 13 nucleotides at the 5′-end of *micF* RNA with positions 120−109 of *ompF*-213 mRNA (forming one turn of a helix) which may facilitate the completion of the second turn of the proposed duplex. Alternatively, it is interesting to note that initial interaction of the RNAs could occur through transient base pairs involving positions 37−39 (UUU) in the loop of *micF* RNA helix I and three unpaired adenine residues (in the stretch of As located at positions 92−85 of *ompF*-213 mRNA) or positions 75−77 (CUC) in the loop of helix II of *micF* RNA and positions 99−97 (GAG) in the loop of *ompF*-213 mRNA helix IA. Similar "kissing interactions" are known to facilitate the hybridization of other antisense RNAs with their targets (Tomizawa, 1984).

A *micF* RNA/*ompF* mRNA duplex structure has been previously proposed (Mizuno et al., 1984; Andersen et al., 1987). Of major interest is that the interaction of the 5′-end segment of *micF* RNA (positions 1−33) with *ompF* mRNA originally proposed is confirmed by the present study; however, we find little support for extended pairing involving positions 37−58 of *micF* RNA with positions 67−87 of *ompF* mRNA as originally proposed.

While the mechanism of *ompF* regulation by *micF* RNA remains unclear, it is known that *micF* RNA binds to and contributes to the chemical destabilization of the *ompF* mRNA. The present study shows that the Shine−Dalgarno sequence and initiator AUG of *ompF* mRNA, found in single-stranded regions in the uncomplexed form of the message, are base-paired to *micF* RNA in the RNA/RNA duplex. This observation is consistent with the idea that *micF* RNA binds to the *ompF* message *in vivo* and blocks translation of OmpF protein. Data from experiments using *micF* RNA expressed from a multicopy plasmid (Andersen et al., 1989) imply that another limiting factor is necessary in order for the *ompF* message to be destabilized. Thus, the mechanism by which *micF* RNA regulates *ompF* mRNA can be viewed as a two-step process. Binding of *micF* RNA to *ompF* mRNA blocks translation (functional inactivation), and then chemical destabilization of the mRNA occurs with the aid of another factor(s). The other necessary factor(s) has not yet been identified, although a protein which specifically binds *micF* RNA, the *micF* RNA-binding protein (Andersen & Delihas, 1990), is a strong candidate. Preliminary data (C. DeLoughery and N. Delihas, unpublished results) suggest that this protein may bind to helix II of *micF* RNA, a region which appears to be structurally similar whether the RNA is free or in the duplex (compare Figures 5 and 6). It is possible that while the hybridized region of the RNA/RNA duplex is responsible for blocking translation of the message, both the loop at *micF* RNA positions 14−20 and hairpin II of *micF* RNA may represent sites of interaction of the complex with this protein or another limiting and necessary factor.

The presence of a stretch of 11 unpaired nucleotides followed by a long stable hairpin at the 5′-end of *ompF* mRNA may be important in regulation of the stability of this RNA. Prokaryotic RNAs without such a 5′-terminal single-stranded region have longer half-lives than those that contain them, and this may be related to the preference of RNase E for a structure containing an unpaired 5′-end (Bouvet & Belasco, 1992). The half-life of *ompF* mRNA has been measured and found to be 4.3 min in the absence of *micF* RNA (unpublished data), while the half-life of *ompA* mRNA (which has no 5′-single-stranded end) is 21 min (Chen et al., 1991). Furthermore, *ompF* mRNA contains several A-U rich regions which resemble sequences known to be recognized by RNase E (Mackie, 1992; McDowall et al., 1994) and seems to be susceptible to degradation by RNase E *in vitro* (unpublished data). While *micF* RNA appears to be the rate-limiting determinant of *ompF* mRNA stability, the above factors imply that the decay of *ompF* mRNA may be at least partially controlled by RNase E. Current work is addressing this possibility.

ACKNOWLEDGMENTS

We thank Dr. Janet Andersen for techniques and discussions throughout the course of this work and Dr. Ann Jacobson and Marie de Crombrugghe for help with the mfold

program. We also thank Dr. Lisa Esterling for construction of plasmid pUCT7micF and Craig DeLoughery for preparation of T7 RNA polymerase. Thanks also go to Dr. Bernard Dudock for the gift of the purified wheat germ 5S RNA and to Dr. John Dunn for help with *in vitro* transcription with T7 RNA polymerase. We extend thanks to Dr. Stanley Fields for critical reading of the manuscript and to Dr. David Williams for discussion and suggestions. We are grateful to Dr. Steven E. Rokita and Dr. Cynthia J. Burrows for their expertise and advice regarding the nickel reagent and to Dr. James Muller for synthesizing the NiCR.

REFERENCES

Aiba, H., Matsuyama, S.-I., Mizuno, T., & Mizushima, S. (1987) *J. Bacteriol. 169*, 3007−3012.
Andersen, J., & Delihas, N. (1990) *Biochemistry 29*, 9249−9256.
Andersen, J., Delihas, N., Ikenaka, K., Green, P. J., Pines, O., Ilercil, O., & Inouye, M. (1987) *Nucleic Acids Res. 15*, 2089−2101.
Andersen, J., Forst, S. A., Zhao, K., Inouye, M., & Delihas, N. (1989) *J. Biol. Chem. 264*, 17961−17970.
Auron, P. E., Weber, L. D., & Rich, A. (1982) *Biochemistry 21*, 4700−4706.
Bouvet, P., & Belasco, J. G. (1992) *Nature 360*, 488−491.
Chen, L.-H., Emory, S. A., Bricker, A. L., Bouvet, P., & Belasco, J. G. (1991) *J. Bacteriol. 173*, 4578−4586.
Chen, X., Rokita, S. E., & Burrows, C. J. (1991) *J. Am. Chem. Soc. 113*, 5884−5886.
Chen, X., Burrows, C. J., & Rokita, S. E. (1992) *J. Am. Chem. Soc. 114*, 322−325.
Chen, X., Woodson, S. A., Burrows, C. J., & Rokita, S. E. (1993) *Biochemistry 32*, 7610−7616.
Chou, J. H., Greenberg, J. T., & Demple, B. (1993) *J. Bacteriol. 175*, 1026−1031.
Cohen, S. P., McMurray, L. M., & Levy, S. B. (1988) *J. Bacteriol. 170*, 5416−5422.
Coyer, J., Andersen, J., Forst, S. A., Inouye, M., & Delihas, N. (1990) *J. Bacteriol. 172*, 4143−4150.
Delihas, N. (1995) *Mol. Microbiol. 15*, 411−414.
Delihas, N., Andersen, J., & Singhal, R. P. (1984) in *Progress in Nucleic Acid Research and Molecular Biology* (Cohn, W. E., & Moldave, K., Eds.) Vol. 31, pp 161−190, Academic Press, Orlando, FL.
Dock-Bregeon, A. C., & Moras, D. (1987) *Cold Spring Harbor Symp. Quant. Biol. 52*, 113−121.
Donis-Keller, H., Maxam, A. M., & Gilbert, W. (1977) *Nucleic Acids Res. 4*, 2527−2538.
Ehresmann, C., Baudin, F., Mougel, M., Romby, P., Ebel, J.-P., & Ehresmann, B. (1987) *Nucleic Acids Res. 15*, 9109−9128.
England, T. E., & Uhlenbeck, O. C. (1978) *Nature 275*, 560−561.
Esterling, L., & Delihas, N. (1994) *Mol. Microbiol. 12*, 639−646.
Fox, G. E., & Woese, C. R. (1975) *Nature 256*, 505−507.
Freier, S. M., Kierzek, R., Jaeger, J. A., Sugimoto, N., Caruthers, M. H., Neilson, T., & Turner, D. H. (1986) *Proc. Natl. Acad. Sci. U.S.A. 83*, 9373−9377.
Gidrol, X., & Farr, S. (1993) *Mol. Microbiol. 10*, 877−884.
Grodberg, J., & Dunn, J. J. (1988) *J. Bacteriol. 170*, 1245−1253.
Hutsul, J., & Worobec, E. (1994) *Microbiology 140*, 379−387.
Inouye, M., & Delihas, N. (1988) *Cell 53*, 5−7.
Jaeger, J. A., Turner, D. H., & Zuker, M. (1989) *Proc. Natl. Acad. Sci. U.S.A. 86*, 7706−7710.
Jaeger, J. A., Turner, D. H., & Zuker, M. (1990) *Methods Enzymol. 183*, 281−306.
Karn, J. L., & Busch, D. H. (1966) *Nature 211*, 160−162.
Lee, R. C., Feinbaum, R. L., & Ambros, V. (1993) *Cell 75*, 843−854.
Lowman, H. B., & Draper, D. E. (1986) *J. Biol. Chem. 261*, 5396−5403.
Mackie, G. A. (1992) *J. Biol. Chem. 267*, 1054−1061.
McDowall, K. J., Lin-Chao, S., & Cohen, S. N. (1994) *J. Biol. Chem. 269*, 10790−10796.
Misra, R., & Reeves, P. R. (1987) *J. Bacteriol. 169*, 4722−4730.
Mizuno, T., Chou, M.-Y., & Inouye, M. (1983) *Proc. Jpn. Acad. 59*, 335−338.
Mizuno, T., Chou, M.-Y., & Inouye, M. (1984) *Proc. Natl. Acad. Sci. U.S.A. 81*, 1966−1970.
Pace, N. R., Smith, D. K., Olsen, G. J., & James, B. D. (1989) *Gene 82*, 65−75.
Ramani, N., Hedeshian, M., & Freundlich, M. (1994) *J. Bacteriol. 176*, 5005−5010.
Romby, P., Moras, D., Bergdoll, M., Dumas, P., Vlassov, V. V., Westhof, E., Ebel, J. P., & Giege, R. (1985) *J. Mol. Biol. 184*, 455.
Rosner, J. L., Chai, T.-J., & Foulds, J. (1991) *J. Bacteriol. 173*, 5631−5638.
Sambrook, J., Fritsch, E. F., & Maniatis, T. (1989) *Molecular Cloning*, Cold Spring Harbor Laboratory Press, Cold Spring Harbor, NY.
Simons, R. W. (1993) in *Antisense Research and Applications* (Crooke, S. T., & Lebleu, B., Eds.) pp 97−124, CRC Press, Ann Arbor, MI.
Sogin, M. L., Ingold, A., Karlok, M., Nielsen, H., & Engberg, J. (1986) *EMBO J. 5*, 3625−3630.
Tetart, F., & Bouche, J.-P. (1992) *Mol. Microbiol. 6*, 615−620.
Tomizawa, J.-I. (1984) *Cell 38*, 861−870.
Turner, D. H., Sugimoto, N., Jaeger, J. A., Longfellow, C. E., Freier, S. M., & Kierzek, R. (1987) *Cold Spring Harbor Symp. Quant. Biol. 52*, 123−133.
Turner, D. H., Sugimoto, N., & Freier, S. M. (1988) *Annu. Rev. Biophys. Biophys. Chem. 17*, 167−192.
Yanisch-Perron, C., Vieira, J., & Messing, J. (1985) *Gene 33*, 103.
Zuker, M. (1989) *Science 244*, 48−52.
Zuker, M. (1994) in *Methods in Molecular Biology, Vol. 25: Computer Analysis of Sequence Data, Part II* (Griffin, A. M., & Griffin, H. G., Eds.), pp 267−294, Humana Press, Totowa, NJ.

BI942634M